IEEE Access
Multidisciplinary | Rapid Review | Open Access Journal

SPECIAL SECTION ON INTEGRATIVE COMPUTER VISION AND MULTIMEDIA ANALYTICS

Received January 30, 2020, accepted February 20, 2020, date of publication February 24, 2020, date of current version March 9, 2020.

Digital Object Identifier 10.1109/ACCESS.2020.2976132

A Coarse-to-Fine Generalized-ICP Algorithm With Trimmed Strategy

XIN WANG, YUN LI, YAXIN PENG, AND SHIHUI YING, (Member, IEEE)
Department of Mathematics, School of Science, Shanghai University, Shanghai 200444, China

Corresponding author: Yaxin Peng (yaxin.peng@shu.edu.cn)

This work was supported in part by the National Natural Science Foundation of China under Grant 11771276, Grant 11971296, and Grant 11871327, and in part by the Capacity Construction Project of local universities in Shanghai under Grant 18010500600.

ABSTRACT In this paper, we introduce a modified Generalized Iterative Closest Point (GICP) algorithm by presenting a coarse-to-fine strategy. Our contributions can be summarized as: Firstly, we use adaptively a plane-to-plane probabilistic matching model by gradually reducing the neighborhood range for given two point sets. It is an inner coarse-to-fine iteration process. Secondly, we use an outer coarse-to-fine strategy to bridge the point-to-point and plane-to-plane registration for refining the matching. Thirdly, we use the trimmed method to gradually eliminate the effects of incorrect correspondences, which improves the robustness of the methods especially for the low overlap cases. Moreover, we also extend our method to the scale registration case. Finally, we conduct extensive experiments to demonstrate that our method is more reliable and robust in various situations, including missing points, noise and different scale factors. Experimental results show that our approach outperforms several state-of-the-art registration methods.

INDEX TERMS Registration, modified GICP, trimmed method.

I. INTRODUCTION

In recent years, with the rapid development of artificial intelligence and autonomous driving, the point set registration is becoming more and more popular. The point set registration problem aims to find the correspondence and transformation between two point sets, and transform one point set to its counterpart through accurate mapping [1]–[5].

Iterative Closest Point (ICP) [6], [7] is a classical point set registration algorithm via alternate iteration to search the correspondence and update the transformation. ICP algorithms of point-to-point and point-to-plane versions are both widely used for their simplicity and effectiveness. In practical applications, however, ICP still has many limitations. The prominent problem is the uncertain correspondence and the failure often induced by sampling, occlusion, outliers, missing or noisy data.

To overcome this shortcoming, many methods have been developed. Zhang proposed an outlier rejection strategy for the correspondence via the distance threshold [8]. It can tick out some unmatched point pairs and outside overlap regions induced by obstructing, missing and outliers. Meanwhile, it is hard to solve the uncertain corresponding problem caused by discretized sampling via the point-to-point based method.

The associate editor coordinating the review of this manuscript and approving it for publication was Guitao Cao.

So some point-to-plane and plane-to-plane based methods were introduced [1], [7], [9]. Among these, Generalized-ICP (GICP) [1] proposed a framework by minimizing the plane-to-plane distance. In addition, the point-to-point based and point-to-plane ICP algorithm can also be viewed as a special case of the GICP framework. Intuitively, they assume that the data are locally planar; thus the searching regions to the closest correspondences are wider than that of the standard point-to-point ICP. So, plane-to-plane ICP obviously improves the robustness against measurement noise.

Then, many modified plane-to-plane ICP methods have been widely used for point cloud data alignment. Visual features and descriptors are introduced into the plane-to-plane error metric [10], [11]. Han *et al.* proposed a hierarchical searching scheme for multi-resolution data to improve the robustness with respect to the local minimum [12], [13].

However, GICP took the trade-off between the accuracy and the robustness for measurement noise. We observe that the final plane-to-plane distance cannot reach as low as the point-to-point ICP. Secondly, GICP is also sensitive to the initial position and thus only achieves local minimum. Thirdly, noise, occlusion and missing points will often make GICP fail to align.

Compared with GICP [1], the principal component analysis (PCA) pays more attention to global distribution. PCA uses the Singular Value Decomposition (SVD) method [14]

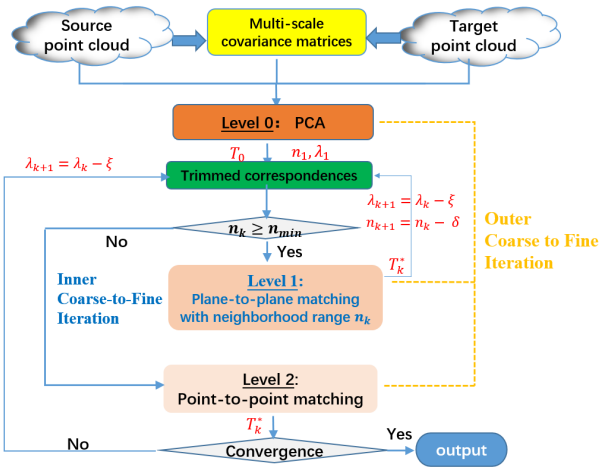

FIGURE 1. Flowchart of the proposed coarse-to-fine framework. This is an inner and outer combined coarse-to-fine algorithm to balance the tradeoff between the accuracy and the robustness to noise.

to obtain several principal axes of two point sets, then aligns the centers and their principal axes [15]. This process can give a better initial rigid transformation, even scale mapping. It can be viewed as the roughest registration strategy.

To solve the problem of the local minimum caused by missing and noise degeneration, Trimmed ICP (TrICP) [16] was proposed, which ticks out outliers and then conducts ICP by minimizing the Trimmed Squared Distance (TSD). On this base, improved TrICP algorithms appeared by introducing an objective function to estimate the overlap rate [17], [18]. Then, Peng *et al.* [19], Dong *et al.* [20] extended this trimmed strategy to the nonrigid transformation. Du *et al.* [21], [22] proposed an ICP algorithm based on the probability or correntropy for precise registration with outliers and noise. Empirically, these methods can significantly improve the performance in a variety of noise degenerations. However, these methods only concern the point-to-point registration problem.

In this paper, we use a coarse-to-fine algorithm combining the inner and outer method to balance the trade-off between the accuracy and the robustness to noise. The inner coarse-to-fine GICP algorithm starts with a wide range of plane-to-plane matching, and the range decreases gradually during each iteration, which is less sensitive to the initial position and more robust to measurement noise, while the outer coarse-to-fine strategy bridges the point-to-point and plane-to-plane registration for refining the matching, which can further improve the accuracy. Moreover, we also propose an adaptive pruning to reject incorrect correspondence in this process, which can avoid the local minimum at the low overlap case caused by missing points and outliers. Finally, we also consider extending the GICP from the rigid to the scale transformation. The basic framework is illustrated in Fig. 1.

This paper is organized as follows. In Section II we introduce the related work, which includes GICP algorithm and the trimmed strategy. Then, we describe our methodology and algorithm in Section III. In Section IV, we introduce the scale stretch version of our method. Experiments and analysis are shown in Section V. Section VI concludes the paper.

II. RELATED WORKS

Given two point sets, the source set $X = \{\boldsymbol{x}_i | i = 1, \ldots, m\}$ and the target set $Y = \{\boldsymbol{y}_j | j = 1, \ldots, l\}$, our aim is to find the best transformation T matching X to Y.

A. GICP ALGORITHM

The GICP algorithm proposed a plane-to-plane registration method based on the Mahalanobis distance, i.e.,

$$T^* = \arg\min_T \sum_{i=1}^{M} \boldsymbol{d}_i^\top M_i \boldsymbol{d}_i \tag{1}$$

where

$$\boldsymbol{d}_i = T \cdot \boldsymbol{x}_i - \boldsymbol{y}_{c(i)}$$
$$M_i = (C_{n,c(i)}^Y + R C_{n,i}^X R^\top)^{-1}.$$

Here $\boldsymbol{d}_i$ is the corresponding Euclidean distance vector between $T \cdot \boldsymbol{x}_i$ and $\boldsymbol{y}_{c(i)}$, $c(i)$ represents the index of the nearest point in Y corresponding to $\boldsymbol{x}_i$, $C_{n,i}^X$ and $C_{n,c(i)}^Y$ are covariance matrices calculated by n closest neighborhood points around $\boldsymbol{x}_i \in X$ and n closest neighborhood points around $\boldsymbol{y}_{c(i)} \in Y$, and R is the rotation.

To model the plane structure, [1] modified the covariance matrix as:

$$C_{n,i}^X = U_{\boldsymbol{x}_i} \begin{pmatrix} 1 & 0 & 0 \\ 0 & 1 & 0 \\ 0 & 0 & \epsilon \end{pmatrix} U_{\boldsymbol{x}_i}^\top \tag{2}$$

$$C_{n,c(i)}^Y = U_{\boldsymbol{y}_{c(i)}} \begin{pmatrix} 1 & 0 & 0 \\ 0 & 1 & 0 \\ 0 & 0 & \epsilon \end{pmatrix} U_{\boldsymbol{y}_{c(i)}}^\top, \tag{3}$$

where $U_{\boldsymbol{x}_i}$ and $U_{\boldsymbol{y}_{c(i)}}$ are obtained by the SVD of the original covariance matrix. Here we assume that the singular values are in descending order, the smallest singular value is replaced by a small constant ϵ, and the remaining two singular values are replaced by 1. When $C_{n,i}^X = \boldsymbol{0}$ and $C_{n,c(i)}^Y = \boldsymbol{I}$, it is equivalent to the standard ICP.

B. TRIMMED STRATEGY

The trimmed strategy updates adaptively the overlap rate r to trim out unmatched points by optimizing the following objective function [17]–[20]:

$$r^* = \arg\min_r \frac{e(r)}{e^\lambda \cdot m \cdot r^\lambda},$$

where $e(r) = \sum_{i=1}^{r \times m} \boldsymbol{d}_i^2$ is the Trimmed square distance (TSD), and λ is a parameter that decreases with iterations.

III. THE PROPOSED COARSE-TO-FINE ITERATIVE MATCHING ALGORITHM

PCA can roughly match point clouds and accelerate the convergence rate, but it may also result in worse initial positions.

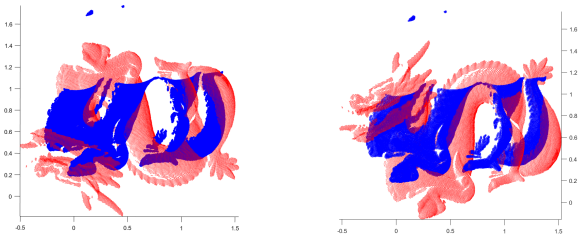

(a) Mirror symmetry (b) After adjustment

FIGURE 2. PCA result. (a) The original PCA result, and (b) The result after reversing axis.

Compared with ICP, GICP considers a plane-to-plane registration model that covers more local information and is less sensitive to the noise. But the proper neighborhood range is hard to determine. Furthermore, we need to trim out the incorrect correspondences for the low overlap data or noising data. By synthesizing the advantages of these methods, we propose a coarse to fine iterative closest point algorithm to deal with these problems. The details of our algorithm are given as follows.

Here we list some notations used in our algorithm. Let $k-1$ be the last iteration, T_k the current transformation consisting of a rotation matrix, a translation vector $\{R_k, \boldsymbol{t}_k\}$, and n_k the updated neighborhood range for the k-th iteration.

A. PREPROCESSING

In this part, we aim to obtain an initial transformation and set some initial parameters. In our algorithm, PCA is used to get the initial transformation T_0 and align two point sets roughly. However, it may cause the mirror symmetry or distribution center difference. In order to avoid the mirror symmetry problem as displayed in Fig. 2(a), we use axis reversal to detect and process as displayed in Fig. 2(b), where the target points are in blue and the source points are in red.

B. ESTIMATING CORRESPONDENCES

Having the transformation T_{k-1} fixed, for each point $\boldsymbol{x}_i \in X$, find its correspondence point $\boldsymbol{y}_{c(i)} \in Y$:

$$c(i) = \arg \min_{j \in \{1,2,\ldots,l\}} \|T_{k-1} \cdot \boldsymbol{x}_i - \boldsymbol{y}_j\|^2. \tag{4}$$

C. CALCULATING THE OVERLAP RATE

Having the correspondences $\{(\boldsymbol{x}_i, \boldsymbol{y}_{c(i)})\}_{i=1}^m$ fixed, compute the squared distances $\{\boldsymbol{d}_{k,i}^2\}_{i=1}^m$

$$\boldsymbol{d}_{k,i}^2 = (T_{k-1} \cdot \boldsymbol{x}_i - \boldsymbol{y}_{c(i)})^\top (T_{k-1} \cdot \boldsymbol{x}_i - \boldsymbol{y}_{c(i)}) \tag{5}$$

and sort them in the ascending order.

Then we calculate the overlap rate according as:

$$r_k = \arg \min_r \sum_{i=1}^{r \times m} \frac{\boldsymbol{d}_{k,i}^2}{e^{\lambda_k} \cdot m \cdot r^{\lambda_k}}, \tag{6}$$

where $\lambda_k = \lambda_{k-1} - \xi$ is a parameter of the trimmed strategy, and the positive constants λ_1 and ξ are defined in advance.

D. UPDATING TRANSFORMATION

In this part, we update the transformation by minimizing the corresponding plane-to-plane distance. We use a large neighborhood range $n_1 = n_{\max}$ as the initial range parameter. In each iteration, the plane scale changes with the number of nearest neighbors.

Here we use $D_{n_k,i}^2$ to represent the plane-to-plane squared distance:

$$D_{n_k,i}^2 = (T \cdot \boldsymbol{x}_i - \boldsymbol{y}_{c(i)})^\top M_{k,i} (T \cdot \boldsymbol{x}_i - \boldsymbol{y}_{c(i)}), \tag{7}$$

where

$$M_{k,i} = (C_{n_k,c(i)}^Y + R C_{n_k,i}^X R^\top)^{-1}, \tag{8}$$

$n_k = n_{k-1} - \delta$ is the updated neighborhood range, and the constant δ is the parameter defined in advance. $C_{n_k,i}^X$ is the modified covariance matrix corresponding to the current n_k nearest points of point $\boldsymbol{x}_i \in X$, $C_{n_k,c(i)}^Y$ is the modified covariance matrix corresponding to the current n_k nearest points of point $\boldsymbol{y}_{c(i)} \in Y$. The covariance matrices are computed by (2) and (3).

We use d_i^2 to represent the point-to-point squared distance:

$$d_i^2 = (T \cdot \boldsymbol{x}_i - \boldsymbol{y}_{c(i)})^\top (T \cdot \boldsymbol{x}_i - \boldsymbol{y}_{c(i)}) \tag{9}$$

Having the correspondences and overlap rate fixed, we can get the Trimmed Mean Square Error (TMSE) for plane-to-plane matching (10)

$$f(T) = \frac{1}{m_r} \sum_{i=1}^{m_r} D_{n_k,i}^2, \tag{10}$$

or point-to-point matching (11):

$$f(T) = \frac{1}{m_r} \sum_{i=1}^{m_r} \boldsymbol{d}_i^2, \tag{11}$$

where m_r is the number of remaining points after trimming, $m_r = r_k \times m$.

For the optimization of transformation, we solve a 6-dimensional vector including rotation angles and translations. If $n_k \geq n_{\min}$, we use the TMSE function (10) and solve the nonlinear optimization problem by the Broyden-Fletcher-Goldfarb-Shanno (BFGS) algorithm [23]–[26], else we solve the TMSE function (11) by SVD [14], since it degenerates into a point-to-point situation when the scale is sufficiently small. Then we update the transformation T_k^*:

$$T_k^* = \arg \min_T f(T). \tag{12}$$

E. SUMMARY OF ALGORITHM

To summarize, our algorithm is listed as Algorithm 1.

Note that at the k-th iteration, before updating transformation, the error is

$$\varepsilon_k := \frac{1}{m_r} \sum_{i=1}^{m_r} \|T_{k-1} \cdot \boldsymbol{x}_i - \boldsymbol{y}_{c(i)}\|^2,$$

Algorithm 1 An Adaptive Generalized-ICP Algorithm

Require: Source set X, target set Y and their multi-scale covariance matrices;
parameters: N_{iter}, $n_{\max}$, $n_{\min}$, δ, $\lambda_{\max}$, ξ;
Ensure: Final transformation T^*;
Initial $n_1 = n_{\max}$, $\lambda_1 = \lambda_{\max}$;
Obtain initial transformation T_0 by PCA.
for iteration $k = 1 : N_{iter}$ **do**
  Estimate correspondences $\{(\boldsymbol{x}_i, \boldsymbol{y}_{c(i)})\}_{i=1}^{m}$ by (4);
  Compute squared distance $\{\boldsymbol{d}_{k,i}^2\}_{i=1}^{m}$ by (5);
  Fix the correspondence, calculate the overlap rate r_k by (6);
  Fix the correspondence and overlap rate, update transformation T_k^* using $D_{n_k,i}^2$ or $\boldsymbol{d}_i^2$;
  if $n_k \geq n_{\min}$ **then**
    optimize the TMSE function (10) via BFGS algorithm;
  else
    solve the TMSE function (11) by SVD;
  end if
  if the stopping condition is satisfied **then**
    break;
  else
    $n_{k+1} = n_k - \delta$;
    $\lambda_{k+1} = \lambda_k - \xi$;
    continue;
  end if
end for

where $m_r = m \times r$. Then, after updating transformation, the new error becomes

$$E_k := \frac{1}{m_r} \sum_{i=1}^{m_r} \|T_k \cdot \boldsymbol{x}_i - \boldsymbol{y}_{c(i)}\|^2.$$

In the algorithm, when any of the following conditions are satisfied, the iteration stops.

1) The maximum iteration number N_{iter} has reached;
2) The mean error E_k is sufficiently small;
3) $|\varepsilon_k - E_k|$ is sufficiently small.

IV. ISOTROPIC SCALE REGISTRATION

In practice, the scale factor is ubiquitous in registration. For example, scanning data from different perspectives and distances may have different scales. In order to match point sets better, besides the rotation and translation, we need to solve a scale parameter. Inspired by [15], [27], [28], to deal with the scale registration, we extend our algorithm to the isotropic scale case.

For the isotropic scale registration problem, the plane-to-plane distance function can be written as:

$$f(s, R, \boldsymbol{t}) = \frac{1}{m_r} \sum_{i}^{m_r} (sR\boldsymbol{x}_i + \boldsymbol{t} - \boldsymbol{y}_{c(i)})^\top M (sR\boldsymbol{x}_i + \boldsymbol{t} - \boldsymbol{y}_{c(i)}), \tag{13}$$

(a) Turbine Blade (b) Dragon (c) Happy Buddha

FIGURE 3. Point cloud data Turbine Blade, Dragon and Happy Buddha.

where s is the isotropic scale factor and M can be computed by (8). Similarly, the point-to-point distance function can be written as:

$$f(s, R, \boldsymbol{t}) = \frac{1}{m_r} \sum_{i}^{m_r} \|sR\boldsymbol{x}_i + \boldsymbol{t} - \boldsymbol{y}_{c(i)}\|^2. \tag{14}$$

When solving this optimization problem, we can add the partial derivative of the scale factor accordingly. The solution to other variables is similar to that mentioned above.

V. EXPERIMENTAL RESULTS AND ANALYSIS

In order to verify the performance of our algorithm, we compare it with other algorithms, i.e., ICP, TrICP and GICP. In addition, the results are also compared with our method using PCA and not using PCA, which are called Adaptive GICP (AGICP) and Modified GICP (MGICP), respectively.

A. DATASETS AND EVALUATION

We use the data Turbine Blade, Dragon and Happy Buddha (Fig. 3) from the Large Geometric Models Archive.[1]

Firstly, the original data are regarded as the source set X, and the target set Y is generated with various transformations, such as rotations from 10 degrees to 40 degrees. Then we add some outliers to the source set. After that, we add some random noise to the source set to generate data in noise condition, or drop some points from the target set to generate data in the missing data condition.

Here we suppose the estimated transformation is $\widetilde{T}$, and the set $X_{\text{trans}} = \widetilde{T} \cdot X$ is obtained by transforming the original source set X. To evaluate our method, we calculate the Root Mean Squared Distance (RMSD) between X_{trans} and the original target set Y.

B. POINT CLOUD REGISTRATION WITHOUT SCALE FACTOR

We perform experiments for Turbine Blade, Dragon and Happy Buddha in two cases: the noise case and the missing data case. In our experiments, we rotate the source data from 10 degrees to 40 degrees. For noise data, we add noise to 50% source points, and add 5% outliers. For missing data, we generate data by dropping 10% to 40% points from the target set and add 5% outliers.

Some visual results are shown in Fig. 4 to Fig. 10, which indicates the registration results for Turbine Blade, Dragon and Happy Buddha in the noise case and in the data

[1] https://www.cc.gatech.edu/projects/large_models/

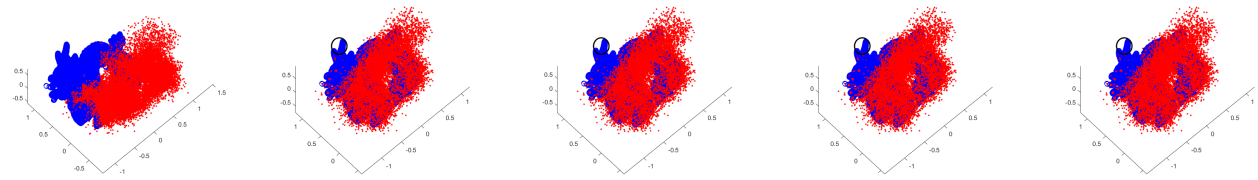

(a) Original point sets (b) GICP (c) TrICP (d) MGICP (e) AGICP

FIGURE 4. Registration results of Dragon data with noise and outliers. (a) 3D view of two point sets before registration; (b) registration result of GICP; (c) registration result of TrICP; (d) registration result of MGICP; (e) registration result of AGICP.

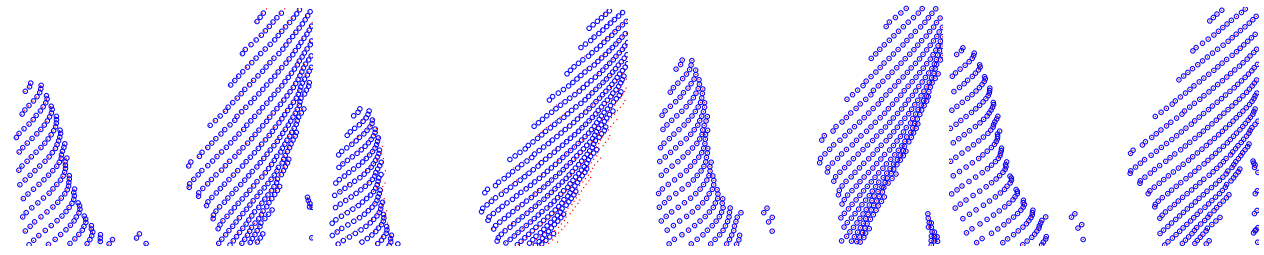

(a) GICP (b) TrICP (c) MGICP (d) AGICP

FIGURE 5. (a), (b), (c) and (d) are the enlarged figures of (b), (c), (d) and (e) in Fig. 4.

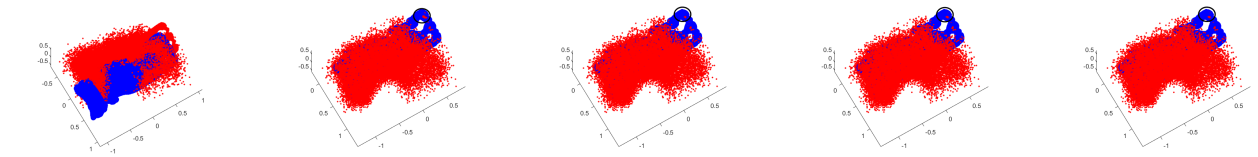

(a) Original point sets (b) GICP (c) TrICP (d) MGICP (e) AGICP

FIGURE 6. Registration results of Happy Buddha data with noise and outliers. (a) 3D view of two point sets before registration; (b) registration result of GICP; (c) registration result of TrICP; (d) registration result of MGICP; (e) registration result of AGICP.

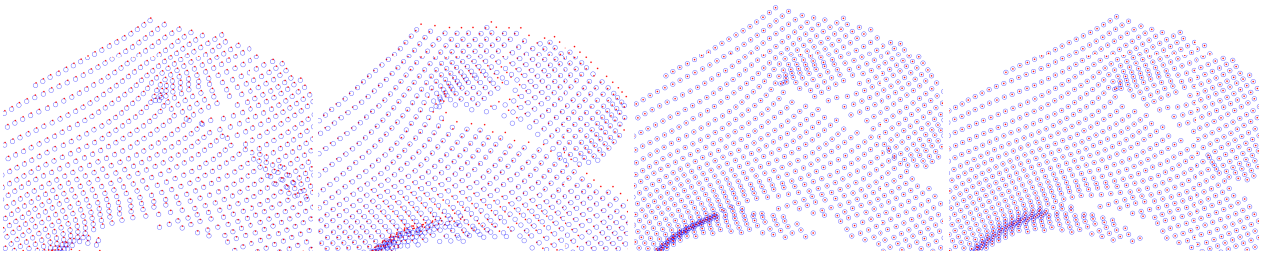

(a) GICP (b) TrICP (c) MGICP (d) AGICP

FIGURE 7. (a), (b), (c) and (d) are the enlarged figures of (b), (c), (d) and (e) in Fig. 6.

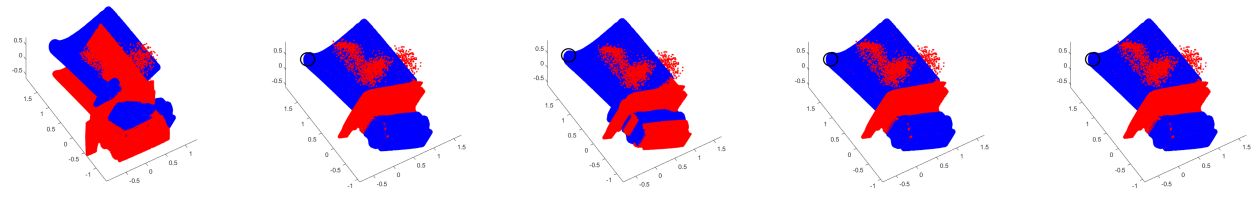

(a) Original point sets (b) GICP (c) TrICP (d) MGICP (e) AGICP

FIGURE 8. Registration results of Turbine Blade data with data missing and outliers. (a) 3D view of two point sets before registration; (b) registration result of GICP; (c) registration result of TrICP; (d) registration result of MGICP; (e) registration result of AGICP.

missing case. In the figures, the source sets are shown in red points and the target sets in blue circles. (a) is the 3D view of point sets before registration. (b), (c), (d) and (e) are the 3D views of four algorithm's results.

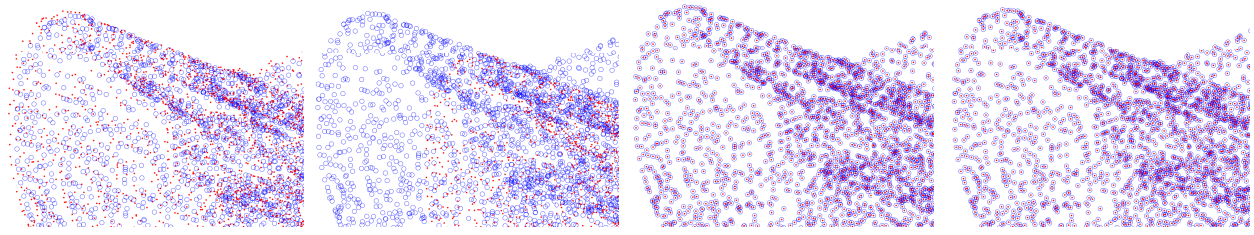

(a) GICP (b) TrICP (c) MGICP (d) AGICP

FIGURE 9. (a), (b), (c) and (d) are the enlarged figures of (b), (c), (d) and (e) in Fig. 8.

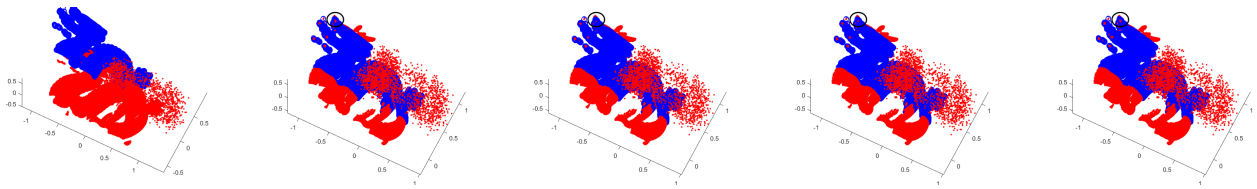

(a) Original point sets (b) GICP (c) TrICP (d) MGICP (e) AGICP

FIGURE 10. Registration results of Dragon data with data missing and outliers. (a) 3D view of two point sets before registration; (b) registration result of GICP; (c) registration result of TrICP; (d) registration result of MGICP; (e) registration result of AGICP.

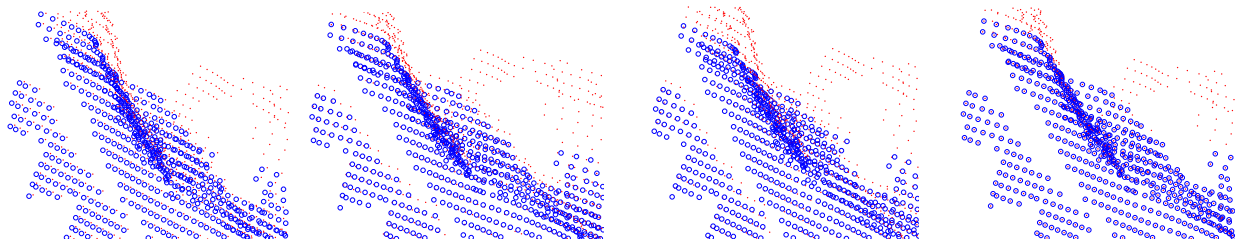

(a) GICP (b) TrICP (c) MGICP (d) AGICP

FIGURE 11. (a), (b), (c) and (d) are the enlarged figures of (b), (c), (d) and (e) in Fig. 10.

TABLE 1. The result of RMSD error and iteration numbers for point cloud without scale factor.

Data	Data case	ICP		GICP ($n = 30$)		TrICP ($\lambda = 9$)		MGICP		AGICP	
		RMSD	Iters	RMSD	Iters	RMSD	Iters	RMSD	Iters	RMSD	Iters
Turbine Blade	missing data	0.1206	97.18	0.0275	16.09	0.0258	64.61	0.0148	21.73	0.0098	20.75
	noise	0.0191	75.24	0.0007	13.93	3.73E-06	50.69	3.65E-06	16.97	3.16E-06	15.07
Dragon	missing data	0.0554	68.63	0.0259	21.29	0.0032	96.11	9.51E-05	18.21	1.94E-06	14.09
	noise	0.0203	70.87	0.0022	18.49	0.0008	62.83	1.64E-06	17.41	2.22E-06	14.52
Happy Buddha	missing data	0.0814	81.08	0.0553	26.77	0.0126	157.67	0.0070	33.16	0.0044	20.94
	noise	0.0331	74.23	0.0017	22.37	0.0031	171.36	1.66E-06	17.92	1.89E-06	14.40

Figs. 4 and 6 illustrate the registration results for Dragon and Happy Buddha in the noise case. For data in Figs. 4 and 6, we add noise to 40% source points, and add 5% outliers. All four algorithms perform well in the noise condition. However, when we enlarge the area marked by the black circle (Figs. 5 and 7), our methods are better than other three algorithms.

Figs. 8 and 10 illustrate the registration results for Turbine Blade and Dragon in the data missing case. For data in Fig. 8, we drop 30% points from the target set and add 5% outliers to source points. For data in Fig. 10, we drop 40% points from the target set and add 5% outliers to source points. Due to the low overlap rate, Turbine Blade data, GICP and TrICP all fail in matching. Contrary to these algorithms, our approach performs very well, which can be viewed in the enlarged figures (Figs. 9 and 11). Fig. 11 shows that our method with PCA is better than that of without PCA.

Statistical results are shown in Table 1 and Figs. 12 and 13. As shown in the table, our method almost gets the smallest RMSD errors of all the datasets no matter in the noise case or in the missing data case, which indicates that our algorithm performs consistently better than ICP, GICP, and TrICP.

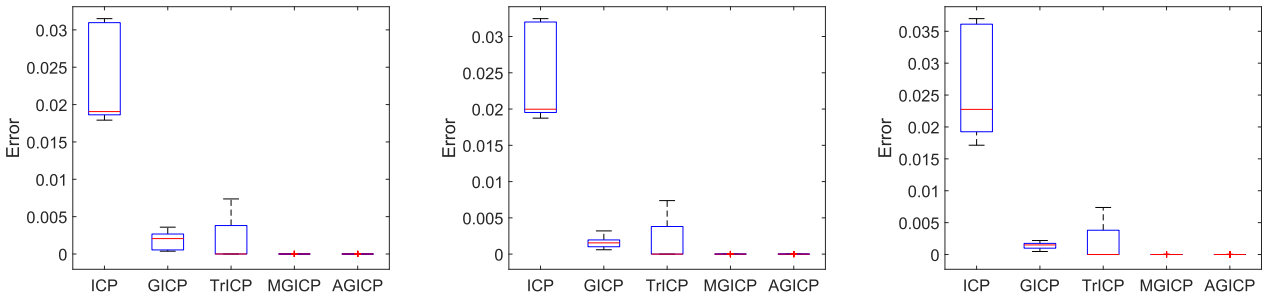

(a) $\sigma^2 = 0.01^2$ (b) $\sigma^2 = 0.05^2$ (c) $\sigma^2 = 0.1^2$

FIGURE 12. Boxplot of RMSD error in various noise cases.

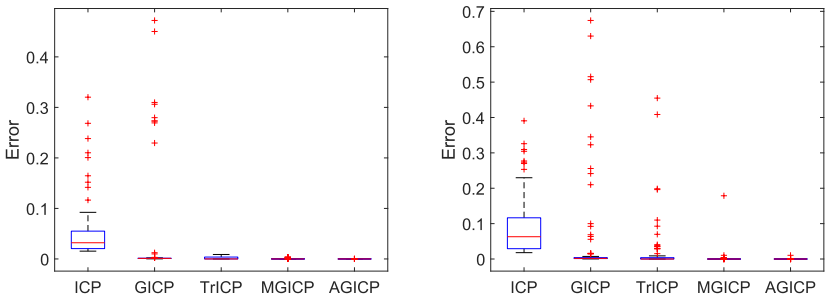

(a) Overlap 80% (b) Overlap 70%

FIGURE 13. Boxplot of RMSD error in various missing data cases.

Table 1 shows that the results of our method with or without PCA nearly have no difference in the noise case, but the result with PCA will be better in the missing data case. The average number of iterations with PCA is about 16, and the average number of iterations is about 21 without PCA, which is lower than ICP, GICP and TrICP. It illustrates that our method converges faster.

In Figs. 12 and 13, we use boxplots to illustrate the RMSD error for all data in Table 1. The boxplot can be interpreted as: the $x-$axis represents four algorithms; $y-$axis represents their respective errors; on each box, the central red mark indicates the median, and the bottom and top edges of the box indicate the 25th and 75th percentiles, respectively; the whiskers extend to the most extreme data points not considered outliers, and the outliers are plotted individually using the red '+' symbol.

Fig. 12(a) to Fig. 12(c) are the results for data in various noise situations. When the noise is small, due to the outliers, ICP gets a bad result, GICP and TrICP get results with some errors, and our results with or without PCA get a small RMSD error. With the increment of noise, the error of ICP becomes higher, but our results are still small. It indicates that our method is robust to noise.

Figs. 13(a) and 13(b) are the results for data in various overlap situations. When the overlap rate is 80%, the errors of TrICP and our method are all small, compared with the higher error in ICP and more abnormal results in GICP. As the overlap rate decreases, the abnormal results of ICP, GICP and TrICP increase, while our method obtains more stable results, which illustrates that our method is robust to missing data.

The boxplot figures reveal that our methods, no matter with or without PCA, nearly get the similar results in the noise case; but in the missing data case, AGICP gets higher error results.

We also compare the convergence rates of these algorithms. We measure the convergence by the Root-Mean-TSD (RMTSD) between Y and $X_{\text{trans}} = T_k \cdot X$ in every iteration. The RMTSD error is defined as

$$\sqrt{\frac{1}{m_r}\sum_{i}^{m_r} \|T_k \cdot \boldsymbol{x}_i - \boldsymbol{y}_{c(i)}\|^2}.$$

Figs. 14 and 15 display the RMTSD error and the overlap rates of data illustrated in Figs. 4, 6, 8 and 10. In Fig. 14, GICP converges fast, but easily falls into local minima, while ICP and TrICP converges slowly. Our method accelerates the convergence procedure by PCA, uses the multi-scale plane matching in the early stage to avoid falling into the local minima, and refines the results by point-to-point matching in the later stage. Figs. 15, (a), (b), (d) show that TrICP and

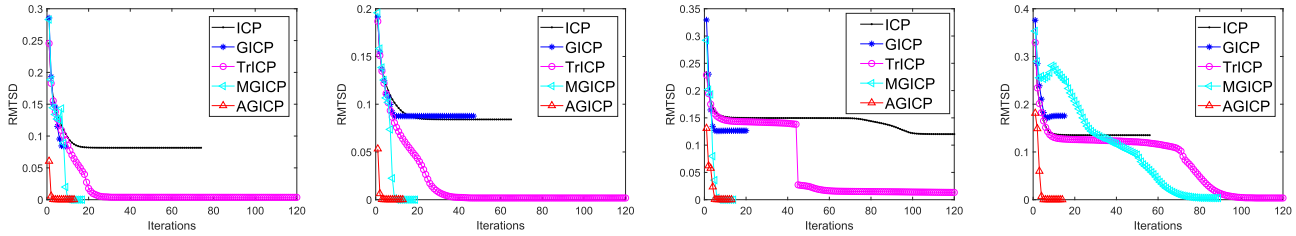

(a) Dragon with noise (b) Happy Buddha with noise (c) Turbine Blade with data missing (d) Dragon with data missing

FIGURE 14. RMTSD error for every iteration of ICP, GICP, TrICP, MGICP and AGICP, (a) is Dragon Data, (b) is Happy Buddha data with noise in Figs. 4 and 6. (c) is Turbine Blade data, and (d) is Dragon Data with data missing in Figs. 8 and 10.

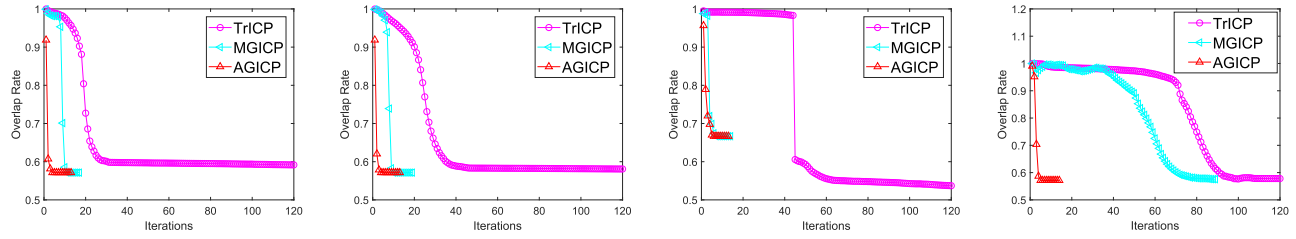

(a) Dragon with noise (b) Happy Buddha with noise (c) Turbine Blade with data missing (d) Dragon with data missing

FIGURE 15. The estimation of the overlap rate for every iteration of TrICP, MGICP and AGICP for experiments in Fig. 14(a)-(d) corresponding to the same data set. Their corresponding groundtruth of overlap rate are about 0.57, 0.57, 0.66 and 0.57.

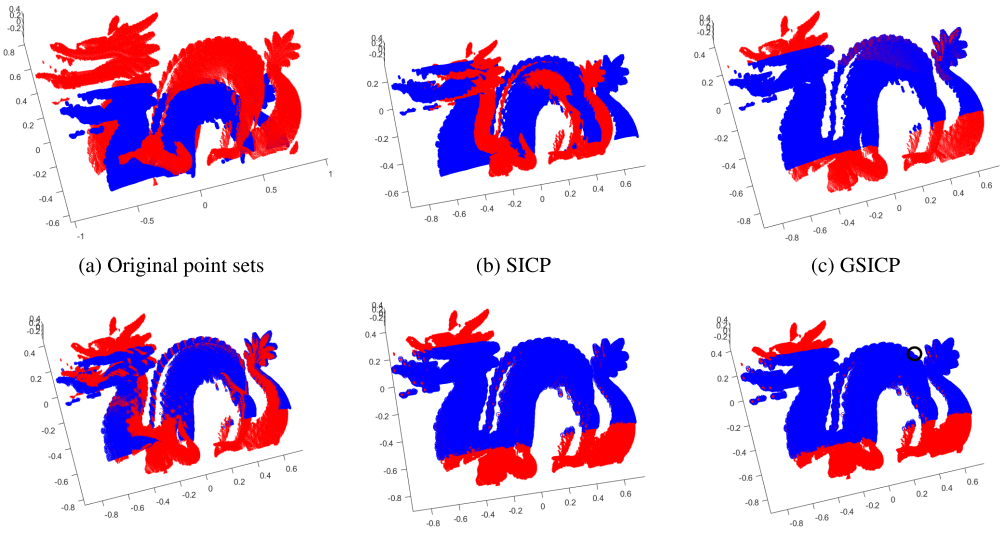

(a) Original point sets (b) SICP (c) GSICP

(d) TrSICP (e) MGICP (f) AGICP

FIGURE 16. Registration results of Dragon data with missing data. (a) 3D view of two point sets before registration; (b) registration result of SICP; (c) registration result of GSICP; (d) registration result of TrSICP; (e) registration result of MGICP; (f) registration result of AGICP.

our method with or without PCA all get good overlap rate results. Fig. 15(c) shows that there is a little deviation in the overlap rate of TrICP; as seen from Fig. 14, the RMTSD error of TrICP achieves significantly small at last, but according to the registration result, the final matching result is biased, because TrICP gets a wrong overlap rate and retains the incorrect matching pairs only according to the distance from point to point. Our method can achieve a better result by plane matching, which reduces the risk of mismatching.

C. POINT CLOUD REGISTRATION WITH ISOTROPIC SCALE FACTOR

In this part, we conduct experiments for data at various scales, from 0.9 to 0.6. At the same time, we also generate datasets with noise and missing data.

We add the isotropic scale factor into the original ICP, TrICP and GICP to generate SICP, TrSICP and GSICP, and solve the registration problems by using SVD method for ICP and TrICP, using BFGS method for GICP.

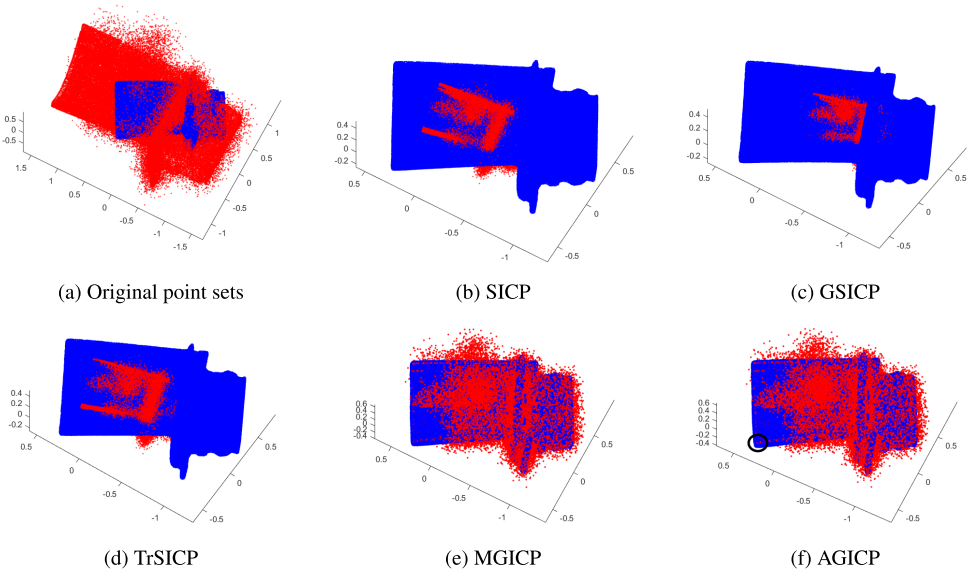

(a) Original point sets (b) SICP (c) GSICP

(d) TrSICP (e) MGICP (f) AGICP

FIGURE 17. Registration results of Turbine Blade data with noise and outliers. (a) 3D view of two point sets before registration; (b) registration result of SICP; (c) registration result of GSICP; (d) registration result of TrSICP; (e) registration result of MGICP; (f) registration result of AGICP.

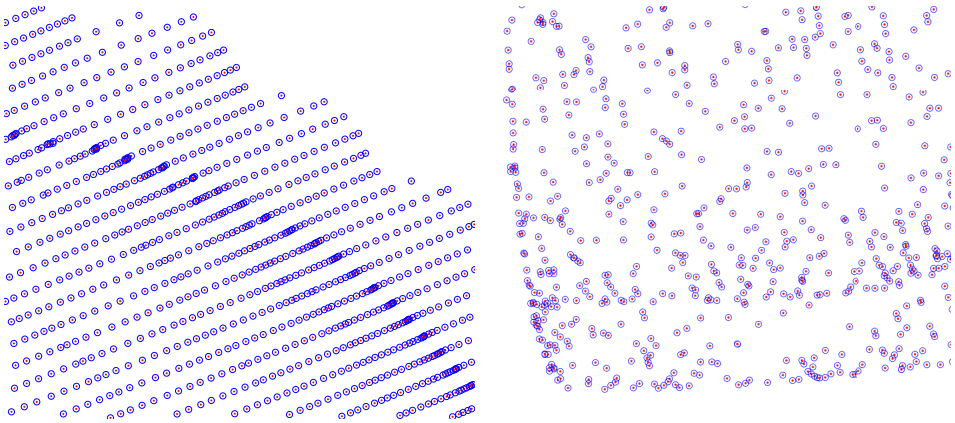

(a) Dragon (b) Turbine Blade

FIGURE 18. Local area enlarged figure for Figs. 16(f) and 17(f).

Some visual results are shown in Figs. 16 and 17, which indicates the registration results for Turbine Blade and Dragon in noise case or in data missing case. In the figures, the source sets are shown in red points and the target sets in blue circles. (a) is the 3D view of point sets before registration. (b), (c), (d), (e) and (f) are the 3D views of registration results of SICP, GSICP, TrSICP [19], [20], MGICP and AGICP.

Figs. 16 and 17 illustrate the registration results for Dragon in the scale registration with missing data and Turbine Blade in scale registration with noise. For data in Fig. 16, we drop 30% points from the target set, and expand the source data so that target data is 0.9 times the source data. For data in Fig. 17, we add noise to 40% source points, add 5% outliers and expand source data so that target data is 0.6 times source data. SICP and TrSICP all trap in the local minima. On the contrary, our method matches the two point sets with a correct scale, and performs very good, which can be further observed by enlarging the area marked by the black circle of our results in Figs. 18(a) and 18(b).

Statistical results are shown in Table 2 and Fig. 19. In the table, from the RMSD error result, ICP, GICP and TrICP cannot deal with scale registration well without considering the scale factor. Our method almost obtains the best result, no matter with or without PCA method. SICP and TrSICP need to iterate many steps to achieve the convergence, and the results are not satisfactory. On the contrary, our results show that the convergence can be achieved in a small number of iterations, and with the PCA method, we obtain more accurate results.

TABLE 2. The result of RMSD error and iteration numbers for point cloud with scale factor.

Method	Turbine Blade		Dragon		Happy Buddha	
	RMSD	Iters	RMSD	Iters	RMSD	Iters
ICP	0.232	61.15	0.156	49.79	0.146	50.83
GICP	0.249	71.13	0.171	30.45	0.151	32.38
TrICP	0.236	197.04	0.162	195.04	0.171	196.42
SICP	0.296	162.09	0.117	135.33	0.095	107.66
GSICP	0.114	43.45	0.029	19.39	0.074	26.98
TrSICP	0.214	180.31	0.044	118.81	0.007	92.24
MGICP	0.010	23.03	**2.04E-03**	18.39	0.007	21.80
AGICP	**3.53E-03**	17.76	**4.05E-03**	14.56	**8.26E-07**	17.45

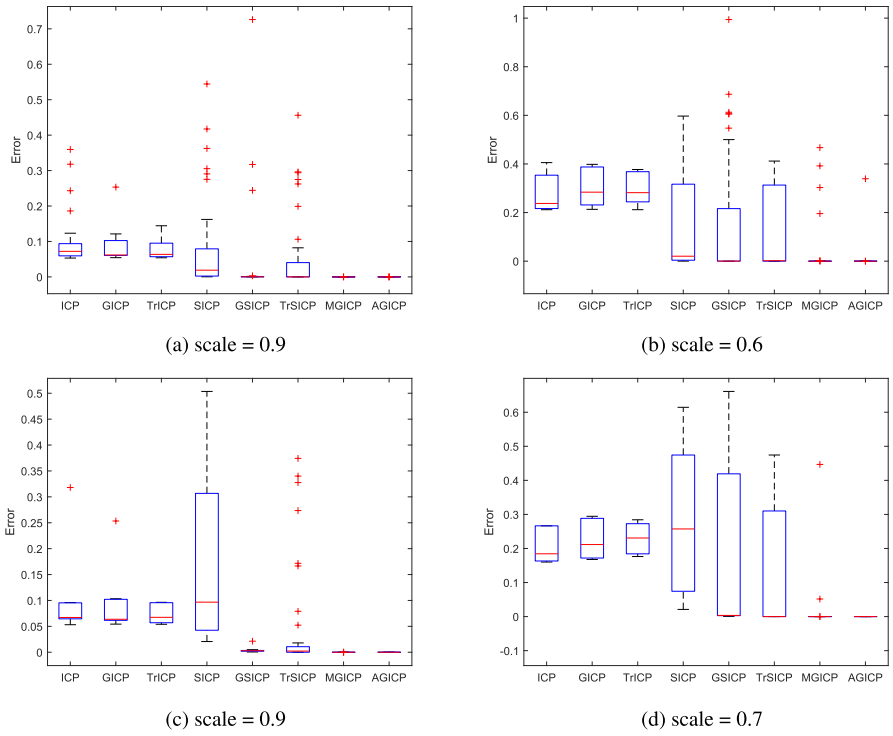

(a) scale = 0.9 (b) scale = 0.6

(c) scale = 0.9 (d) scale = 0.7

FIGURE 19. Boxplot of RMSD error in various scale cases. (a) and (b) are the results for data with missing data, (c) and (d) are the results for data with noise.

Fig. 19(a) to Fig. 19(d) are the results for data in various scale situations with noise or missing data. Original ICP, TrICP and GICP obviously fail to match because they do not take the scale into account. SICP and TrSICP may fail in the scale registration, and get higher error with the scale decreasing. GSICP obtains the results with a low average error but not robust, and our method gets stable results at different scale factors no matter with PCA method or not.

In Figs. 20 and 21 we display the RMTSD error and the overlap rate. For the scale registration, SICP and TrSICP get high RMTSD errors, TrSICP also has a wrong overlap rate, which almost takes all points into account. GSICP gets a very small RMTSD error as the scale parameter decreases, but it is a degenerate case. Because GSICP and our method initially calculate the plane-to-plane distance, and our method calculates the point-to-point distance in the later stage, which causes some fluctuations in our RMTSD results. After PCA preprocessing, our method has greatly improved the calculation of scale and the overlap rate, so the correct convergence results can be obtained quickly.

Our method gets an initial position after PCA, uses multi-scaled plane-to-plane matching and trimmed method to reject the influence of incorrect correspondences, and refines the result by point-to-point matching finally. For the experimental data, no matter what random noise, isotropic scale factor, or the overlap rate in various rotation, our algorithm

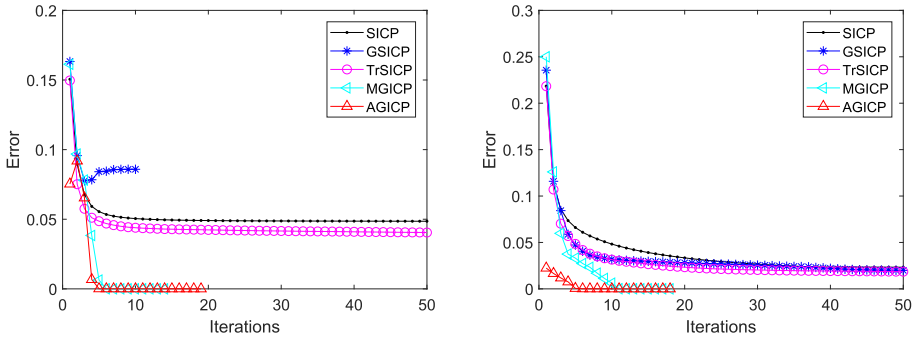

(a) Dragon with data missing (b) Turbine Blade with noise

FIGURE 20. RMTSD error for every iteration of SICP, GSICP, TrSICP, MGICP and AGICP, (a) is Dragon data, (b) is Turbine Blade in Fig. 16 and Fig. 17.

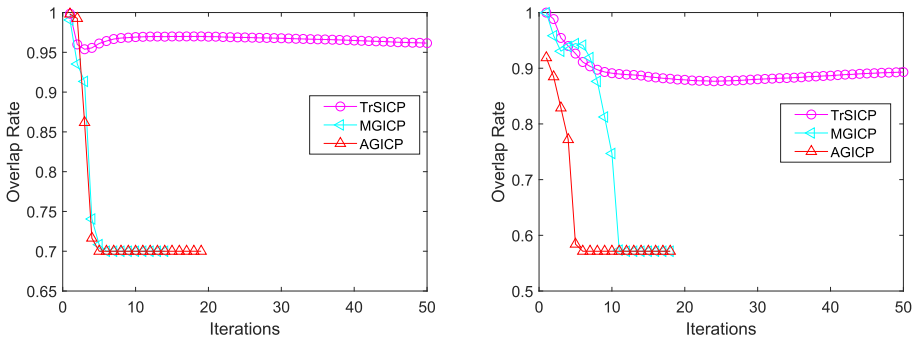

(a) Dragon with data missing (b) Turbine Blade with noise

FIGURE 21. overlap rate for every iteration of TrSICP, MGICP and AGICP, (a) is Dragon data, (b) is Turbine Blade in Figs. 16 and 17. Their corresponding groundtruth of overlap rate are about 0.7 and 0.57.

TABLE 3. The result of RMSD error and runtime comparison for Figs.4, 6 and 8.

Method	Turbine Blade		Dragon		Happy Buddha	
	RMSD	Time(s)	RMSD	Time(s)	RMSD	Time(s)
GICP	0.0015	3.817	0.0017	1.458	0.0018	9.704
TrICP	0.1986	20.47	0.0073	13.29	0.0038	33.42
MGICP	**2.8E-06**	5.228	**2.3E-06**	4.414	**1.0E-06**	12.00
AGICP	**2.4E-06**	4.021	**1.9E-06**	2.016	**8.2E-07**	7.377

can achieve satisfactory results. Experimental results demonstrate that our method is robust to noise and missing data.

In addition, we add the computation time comparison results in Table 3. The experimental results show that the run time of AGICP is much less than that of point-to-point methods, and comparable to GICP.

VI. CONCLUSION

In this paper, we have proposed a coarse to fine iterative closest point algorithm by introducing a modified multi-scale GICP algorithm to refine the matching accuracy, especially for low overlap cases. We have adopted a multi-scale plane-to-plane matching by using a gradually reduced neighborhoods range, and trimmed method to reject the influence of incorrect correspondences. The extensive experiments demonstrate that our algorithm is more accurate and robust in a variety of situations, including missing points and noise.

REFERENCES

[1] A. V. Segal, D. Haehnel, and S. Thrun, "Generalized-ICP," *Robot. Sci., Syst.*, vol. 2, no. 4, p. 435, Jun. 2009.

[2] J. Ma, J. Wu, J. Zhao, J. Jiang, H. Zhou, and Q. Z. Sheng, "Nonrigid point set registration with robust transformation learning under manifold regularization," *IEEE Trans. Neural Netw. Learn. Syst.*, vol. 30, no. 12, pp. 3584–3597, Dec. 2019.

[3] J. Ma, J. Zhao, J. Jiang, H. Zhou, and X. Guo, "Locality preserving matching," *Int. J. Comput. Vis.*, vol. 127, no. 5, pp. 512–531, Sep. 2018.

[4] J. Ma, J. Zhao, and A. L. Yuille, "Non-rigid point set registration by preserving global and local structures," *IEEE Trans. Image Process.*, vol. 25, no. 1, pp. 53–64, Jan. 2016.

[5] J. Ma, W. Qiu, J. Zhao, Y. Ma, A. L. Yuille, and Z. Tu, "Robust L_2E estimation of transformation for non-rigid registration," *IEEE Trans. Signal Process.*, vol. 63, no. 5, pp. 1115–1129, Mar. 2015.
[6] P. J. Besl and N. D. McKay, "A method for registration of 3-D shapes," *IEEE Trans. Pattern Anal. Mach. Intell.*, vol. 14, no. 2, pp. 239–256, Feb. 1992.
[7] Y. Chen and G. Medioni, "Object modelling by registration of multiple range images," *Image Vis. Comput.*, vol. 10, no. 3, pp. 145–155, Apr. 1992.
[8] Z. Zhang, "Iterative point matching for registration of free-form curves and surfaces," *Int. J. Comput. Vision*, vol. 13, no. 2, pp. 119–152, Jul. 1992.
[9] J. Serafin and G. Grisetti, "NICP: Dense normal based point cloud registration," in *Proc. IEEE/RSJ Int. Conf. Intell. Robots Syst. (IROS)*, Sep. 2015, pp. 742–749.
[10] G. Pandey, S. Savarese, J. R. McBride, and R. M. Eustice, "Visually bootstrapped generalized ICP," in *Proc. IEEE Int. Conf. Robot. Autom.*, May 2011, pp. 2660–2667.
[11] M. Korn, M. Holzkothen, and J. Pauli, "Color supported generalized-ICP," in *Proc. Int. Conf. Comput. Vis. Theory Appl. (VISAPP)*, vol. 3, Jan. 2014, pp. 592–599.
[12] J. Han, P. Yin, Y. He, and F. Gu, "Enhanced ICP for the registration of large-scale 3D environment models: An experimental study," *Sensors*, vol. 16, no. 2, p. 228, Feb. 2016.
[13] P. Yin, F. Gu, D. Li, Y. He, L. Yang, and J. Han, "GPU-based heuristic escape for outdoor large scale registration," in *Proc. IEEE Int. Conf. Real-Time Comput. Robot. (RCAR)*, Jun. 2016, pp. 260–265.
[14] K. S. Arun, T. S. Huang, and S. D. Blostein, "Least-squares fitting of two 3-D point sets," *IEEE Trans. Pattern Anal. Mach. Intell.*, vol. PAMI-9, no. 5, pp. 698–700, Sep. 1987.
[15] S. Ying, J. Peng, S. Du, and H. Qiao, "A scale stretch method based on ICP for 3D data registration," *IEEE Trans. Autom. Sci. Eng.*, vol. 6, no. 3, pp. 559–565, Jul. 2009.
[16] D. Chetverikov, D. Stepanov, and P. Krsek, "Robust Euclidean alignment of 3D point sets: The trimmed iterative closest point algorithm," *Image Vis. Comput.*, vol. 23, no. 3, pp. 299–309, Mar. 2005.
[17] J. M. Phillips, R. Liu, and C. Tomasi, "Outlier robust ICP for minimizing fractional RMSD," in *Proc. 6th Int. Conf. 3-D Digit. Imag. Model. (3DIM)*, Aug. 2007, pp. 427–434.
[18] S. Du, "Robust iterative closest point algorithm for registration of point sets with outliers," *Opt. Eng.*, vol. 50, no. 8, Aug. 2011, Art. no. 087001.
[19] Y. Peng, S. Ying, J. Qin, and T. Zeng, "Trimmed strategy for affine registration of point sets," *J. Appl. Remote Sens.*, vol. 7, no. 1, Dec. 2013, Art. no. 073468.
[20] J. Dong, Y. Peng, S. Ying, and Z. Hu, "LieTrICP: An improvement of trimmed iterative closest point algorithm," *Neurocomputing*, vol. 140, pp. 67–76, Sep. 2014.
[21] S. Du, J. Liu, C. Zhang, J. Zhu, and K. Li, "Probability iterative closest point algorithm for m-D point set registration with noise," *Neurocomputing*, vol. 157, pp. 187–198, Jun. 2015.
[22] S. Du, G. Xu, S. Zhang, X. Zhang, Y. Gao, and B. Chen, "Robust rigid registration algorithm based on pointwise correspondence and correntropy," *Pattern Recognit. Lett.*, to be published.
[23] C. G. Broyden, "The convergence of a class of double-rank minimization algorithms 1. General considerations," *IMA J. Appl. Math.*, vol. 6, no. 1, pp. 76–90, 1970.
[24] R. Fletcher, "A new approach to variable metric algorithms," *Comput. J.*, vol. 13, no. 3, pp. 317–322, Mar. 1970.
[25] D. Goldfarb, "A family of variable-metric methods derived by variational means," *Math. Comput.*, vol. 24, no. 109, p. 23, Jan. 1970.
[26] D. F. Shanno, "Conditioning of quasi-newton methods for function minimization," *Math. Comput.*, vol. 24, no. 111, p. 647, Sep. 1970.
[27] H. Zha, M. Ikuta, and T. Hasegawa, "Registration of range images with different scanning resolutions," in *Proc. SMC Conf. IEEE Int. Conf. Syst., Man Cybern. 'Cybern. Evolving Syst., Hum., Org., Complex Interact.'*, vol. 2, Oct. 2000, pp. 1495–1500.
[28] S. Du, J. Liu, B. Bi, J. Zhu, and J. Xue, "New iterative closest point algorithm for isotropic scaling registration of point sets with noise," *J. Vis. Commun. Image Represent.*, vol. 38, pp. 207–216, Jul. 2016.

XIN WANG received the B.Sc. degree in mathematics from Nanjing Normal University, Nanjing, China, in 2003, and the Ph.D. degree in mathematics from the Institute of Computational Mathematics and Scientific/Engineering Computing (ICMSEC), Chinese Academy of Sciences, Beijing, China, in 2008. She is currently a Lecturer with the Department of Mathematics, School of Science, Shanghai University, Shanghai, China. Her research interests include multiscale analysis, point cloud, and image processing.

YUN LI is currently pursuing the M.S. degree with the Department of Mathematics, School of Science, Shanghai University. Her research interests include point set registration, computer vision, machine learning, and SLAM.

YAXIN PENG received the B.Sc. degree in mathematics from Anhui Normal University, Wuhu, China, in 2002, the M.Sc. degree in mathematics from East China Normal University (ECNU), Shanghai, China, in 2005, and the Ph.D. degree in mathematics from the Ecole Normale Suprieure de Lyon, Lyon, France, and ECNU, in 2008. She is currently an Associate Professor with the Department of Mathematics, School of Science, Shanghai University, Shanghai. Her research interests include geometric variation, metric learning, point cloud, and image processing.

SHIHUI YING (Member, IEEE) received the B.Eng. degree in mechanical engineering and the Ph.D. degree in applied mathematics from Xi'an Jiaotong University, Xi'an, China, in 2001 and 2008, respectively. He held a postdoctoral position at the Biomedical Research Imaging Center, University of North Carolina at Chapel Hill, Chapel Hill, NC, USA, from 2012 to 2013. He is currently a Professor with the Department of Mathematics, School of Science, Shanghai University, Shanghai, China. His current research interests include geometric theory and methods for medical image processing and machine learning.